A&A 496, 133–137 (2009)
DOI: 10.1051/0004-6361:200810403

Astronomy & Astrophysics

Revisiting the optical interferometry observations of HR 4049⋆ *(Research Note)*

J.-L. Menut[1], O. Chesneau[2], E. Bakker[3], B. Lopez[2], G. Perrin[4], C. Leinert[5], and A. Quirrenbach[6]

[1] Observatoire de la Côte d'Azur, Dpt. Gemini-CNRS-UMR 6203, BP 4229, 06304 Nice, France
e-mail: menut@obs-azur.fr
[2] Observatoire de la Côte d'Azur, Dpt. Gemini-CNRS-UMR 6203, Avenue Copernic, 06130 Grasse, France
e-mail: Olivier.Chesneau@obs-azur.fr
[3] Observatoire de Paris – Section de Meudon, 5 Place Jules Janssen, 92195 Meudon, France
[4] Magdalena Ridge Observatory, New Mexico Tech, 801 Leroy Place, Socorro, NM 87801, USA
[5] Max-Planck-Institut für Astronomie, Königstuhl 17, 69117 Heidelberg, Germany
[6] Zentrum für Astronomie, Landessternwarte, Königstuhl 12, 69117 Heidelberg, Germany

Received 17 June 2008 / Accepted 10 November 2008

ABSTRACT

Aims. We present high spatial resolution observations in the mid-infrared of the dusty core of the binary system HR 4049.
Methods. We used the mid-infrared interferometer MIDI/VLTI with 40 m projected baselines. These observations provided two spectrally dispersed visibility curves at a spatial resolution of ∼10 mas. Acquisition images and spectra are in addition obtained with a single telescope spatial resolution of ∼250 mas.
Results. The MIDI spectra show features due to emission lines (7.9, 8.6 and 11.3 micron) attributed to PAHs. The comparison between ISO and MIDI spectra and dispersed visibility curves allows us to investigate the budget of continuum and PAH emission from distant regions to the inner regions of the compact dusty structure. The flux balance between these different PAH features is different to the one seen in the large beam ISO spectrum, suggesting different contributions at varying locations from the central star for the different PAH species. These features are over-resolved (i.e. their correlated flux is close to zero), placing the bulk of their line forming region at least at 50−70 mas from the central star. The continuum extension is estimated to range between 23 and 27 mas using a Gaussian model, and is very close to the *K*-band sizes measured with VINCI/VLTI, implying that the emitting regions of the near and mid-IR are similar. The visibilities from the two different baselines do not allow us to constrain the shape of the continuum emitting region but noticeable differences between them suggest that the *N* band dusty environment is flattened in a direction that coincides with the one suggested by previous polarimetric observations.

Key words. techniques: interferometric – techniques: high angular resolution – stars: AGB and post-AGB – stars: mass-loss – stars: circumstellar matter

1. Introduction

HR 4049 (HD 89353, AG Ant) is a binary system containing a cool post-AGB star surrounded by a massive and stable circumbinary envelope resulting from mass loss processes during the AGB phase. Together with the famous Red Rectangle, this is an archetype of a very important class of evolved objects exhibiting strong infrared excesses of circumstellar origin from hot dust and signatures of binarity (Van Winckel et al. 2006).

The spectral energy distribution (SED) of HR 4049 exhibits a strong infrared excess that can be fitted almost perfectly with a single blackbody function at $T \sim 1150$ K. On this basis, it has been suggested that the radiation we observe is coming from the inner rim of a circumbinary thick disk heated by the central sources (Dominik et al. 2003). The orbital period of HR 4049 is 430 days (Bakker et al. 1998) and the best distance estimate is from the Hipparcos parallax, ranging from 467 to 1162 pc. In the frame of this model, the inner rim is at 10 AU from the central sources, i.e. covers an angular diameter of 20−40 mas, and the disk inclination is about 60°.

Molster et al. (1996) and Beintema et al. (1996) presented the rich Polycyclic Aromatic Hydrocarbon (PAH) emission band in the SWS/ISO spectra. Among the observed objects, HR 4049 shows remarkable sub-structures in the major bands (among which 8.6 and 11.3 micron) and narrower features that were interpreted as being due to the emission from small, ionized, hydrogen-rich and highly excited PAHs.

HR 4049 was observed with the VINCI instrument of the VLTI (Antoniucci et al. 2005). The measurements, covering an azimuth range of ∼60° for the sky-projected baseline showed only a slight variation of the measured angular values along the different directions sampled.

In the following, we will present the MIDI observations of HR 4049, carried out in 2004 with 2 different baselines (Sect. 2), the description of the reduced data (Sect. 3), the analysis of these results (Sect. 4) with a strong emphasis on the PAH features. We conclude this paper in the final section.

2. Observations

The VLTI/MIDI interferometer combines directly the *N* band light from two telescopes (Leinert et al. 2003a,b; Ratzka 2005; Ratzka et al. 2007). The two observations of HR 4049 analyzed

⋆ Based on observations made with the Very Large Telescope Interferometer at Paranal Observatory.

and discussed in this paper were conducted during the nights of February 4, 2004 and June 2, 2004, and were obtained with the VLT Unit Telescopes (UTs) UT2 and the UT3. These obervations were performed within the scope of the MIDI "Guaranteed Time Observations" (GTO), under varying atmospheric conditions (mean seeing of about 1.22″ and 0.48″ respectively). The data were recorded with two different projected baselines, (40.8 m, 37.1° of azimuthal angle) and (45.4 m, 70.8°).

The data reduction packages MIA and EWS[1] (Leinert et al. 2004; Ratzka 2005; Jaffe 2004; Ratzka et al. 2007) were used to reduce the spectra and visibilities (Chesneau et al. 2005). Chopped acquisition images were recorded (f = 2 Hz, 4 ms per frame, 1000 to 2000 frames, 98 mas per pixel) for the fine acquisition of the target. The default filter is centered at 8.7 μm (1.6 μm wide).

The grism of MIDI was used, providing a spectral dispersion of 260 that can be compared to the spectral dispersion of ISO SWS spectra of the order of 1000. The slit's width was about 0.52″.

The journal of interferometric observations is presented in Table 1.

We used the interferometric calibrator, HD 90432 (K4.5III), as an absolute flux calibrator. It was observed immediately before or after each science target observation. For the intrinsic calibrator spectra we used the spectral template from Cohen et al. (1999) of HD 139127 (K4.5III). No airmass correction was applied, because for each measurement of the source a calibrator (HD 90432) was observed with an airmass difference not exceeding 0.1.

The extraction of the dispersed visibilities is described in Chesneau et al. (2005). The calibrated visibilities are shown in Fig. 1.

The visibilities extracted in this paper are similar to the ones presented by Bakker et al. (2004) from the same dataset, reduced with the EWS software. These data have been processed independently using the two data reduction packages (MIA wich is based on power spectrum analysis and EWS which is based on a shift-and-add algorithm in the complex plane, see Leinert et al. 2004; Ratzka 2005; Jaffe 2004 for more details), indicating a robustness of the data reduction process. Some difficulties were encountered, however, in the reducing process.

First, these grism data were recorded using only a single calibrator with the same instrumental set-up, whereas all other calibrators for the night were observed with the lower-resolution prism. Second the grism images of the two interferometric spectra are distorted on the detector, leading to an additional source of error, and the photometric accuracy can be less accurate. However, the calibrator and the science targets are bright, allowing a good signal to be recorded by pixel. Moreover, the variations of the instrumental contrast, estimated from the numerous calibrators observed with the prism (in low resolution mode) are limited to 8%. We also decided to reduce the files recorded during the search of the fringes, which contains only a few scans with an interferometric signal. The level of the raw visibilities is in agreement with the tracking files, but with a higher pixel-to-pixel noise level. The results obtained with the MIA and EWS packages show good agreement, and we only present the result reduced with the EWS package below. The relative errors of the calibrated visibilities are typically ≈1015% , and the error sources are described in Ohnaka et al. (2007), Ratzka et al. (2007).

[1] http://www.mpia-hd.mpg.de/MIDISOFT/, http://www.strw.leidenuniv.nl/~nevec/MIDI/

Table 1. Journal of observations: MIDI UT2-UT3. Length and position angle of the projected baseline is indicated.

Star	Template	Time	Frames
2004-06-02, B = 40.84 m, Θ = 37.1°, Grism, SCI-PHOT			
HD 90432	00:02:56	Track. dispersed	1200
HD 90432	00:03:49	Track. dispersed	1200
HD 90432	00:04:43	Track. dispersed	1200
HD 90432	00:05:37	Track. dispersed	1200
HD 90432	00:06:31	Track. dispersed	1200
HD 90432	00:07:25	Track. dispersed	1200
HD 90432	00:08:18	Track. dispersed	800
HD 90432	00:13:35	Phot. disp.	1200
HD 90432	00:14:29	Phot. disp.	300
HD 90432	00:16:18	Phot. disp.	1200
HD 90432	00:17:12	Phot. disp.	300
HR 4049	00:48:39	Track. dispersed	1200
HR 4049	00:49:32	Track. dispersed	1200
HR 4049	00:50:26	Track. dispersed	1200
HR 4049	00:51:20	Track. dispersed	1200
HR 4049	00:52:14	Track. dispersed	1200
HR 4049	00:53:08	Track. dispersed	1200
HR 4049	00:54:01	Track. dispersed	800
HR 4049	00:58:29	Phot. disp.	1200
HR 4049	00:59:23	Phot. disp.	300
HR 4049	01:01:12	Phot. disp.	1200
HR 4049	01:02:06	Phot. disp.	300
2004-02-04, B = 45.44 m, Θ = 70.8°, Grism, SCI-PHOT			
HR 4049	03:30:08	Track. dispersed	1200
HR 4049	03:31:01	Track. dispersed	1200
HR 4049	03:31:55	Track. dispersed	1200
HR 4049	03:32:49	Track. dispersed	1200
HR 4049	03:33:43	Track. dispersed	1200
HR 4049	03:37:53	Phot. disp.	1200
HR 4049	03:38:47	Phot. disp.	800
HR 4049	03:40:32	Phot. disp.	1200
HR 4049	03:41:26	Phot. disp.	800
HD 90432	04:04:22	Track. dispersed	1200
HD 90432	04:05:27	Track. dispersed	1200
HD 90432	04:06:33	Track. dispersed	1200
HD 90432	04:07:39	Track. dispersed	1200
HD 90432	04:08:45	Track. dispersed	1200
HD 90432	04:09:51	Track. dispersed	1200
HD 90432	04:10:56	Track. dispersed	800
HD 90432	04:16:40	Phot. disp.	1200
HD 90432	04:17:46	Phot. disp.	800
HD 90432	04:19:28	Phot. disp.	1200
HD 90432	04:20:34	Phot. disp.	800

3. Results

3.1. MIDI and ISO spectra

Figures 2 and 3 show the ISO and MIDI spectra and their respective fit continuum. The ISO spectrum has already been discussed in Beintema et al. (1996). The MIDI continuum at 10 μm represents 67 ± 4% of the ISO spectrum. An other difference between the two spectra is that the PAH features are weaker in the MIDI spectrum when scaled to the ISO one, the reduction in strength between the ISO and MIDI spectra is much more pronounced for the feature at 11.3 μm than for those at 7.9 and 8.6 μm.

The underlying continuum was estimated based on a 5th-order polynomial fit for the ISO spectra and 6th-order fit for the MIDI one. The fit of the ISO spectrum, estimated from a wider continuum range, is more robust. Due to a lack of continuum close to the edge of the atmospheric window at 7.5 μm, we used the local slope of the ISO fit to estimate the MIDI continuum between 7.5 and 9 μm.

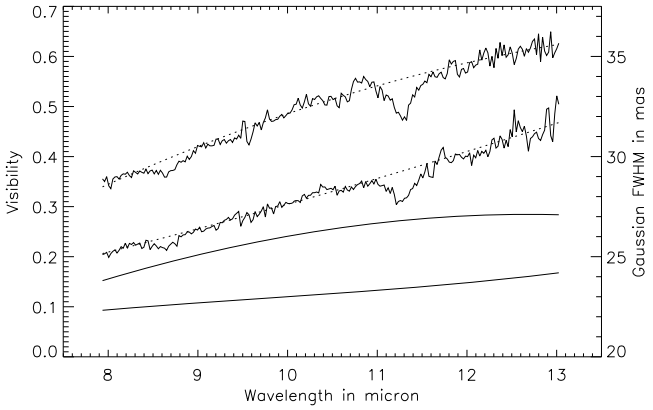

Fig. 1. MIDI dispersed visibility of 2004-06-02 (*top*, baseline: 40.8 m) and 2004-02-04 (*bottom*, baseline: 45.4 m). Using a parabolic fit of these visibilities, a Gaussian *FWHM* is estimated and shown as the two bottom curves (scale on the right), the 2004-02-04 extension being smaller than the one from the 2004-06-02.

In the ISO spectrum, the PAH features peak (see Fig. 3, left) at 47%, 37% and 69% over the continuum at 7.9 μm, 8.6 μm and 11.3 μm respectively, whereas in the MIDI spectrum, these features show respectively a peak up to 25%, 16% and 19% over the continuum. The error bar of the MIDI continuum is given by the standard deviation of three different fits: the first one is the direct fit of the MIDI data, the second one is the fit of the ISO continuum, rescaled to the MIDI level, and the last one is a combination of the first one for the wavelength greater than 9 μm (where the direct fit is better) and of the second one for the wavelength less than 9 μm (where rescaled fit of ISO is better).

The corresponding total flux amount in these features (see Fig. 3, right) is for the ISO spectrum, of 478 Jy, 189 Jy and 220 Jy for the 7.9, 8.6 and 11.3 μm (73 Jy for the small plateau between 8.25 and 8.5 μm). For the MIDI spectrum, it corresponds to 171, 60 and 42 Jy (33 for the plateau).

We evaluated the PAH contribution to about 16 ± 4% of the flux in the MIDI acquisition filter (bandpass shown in Fig. 2). Note that it would have been 29% with the ISO spectrum. The quality of the acquisition images is not good enough to state that the object is more extended than the PSFs recorded soon before and after the observations of HR 4049, but the source images appear essentially unresolved.

3.2. MIDI visibilities

The dusty environment of HR 4049 is well resolved by MIDI with 40−45 m baseline. The visibility curves increase with wavelengths from ∼0.2−0.3 at 8 μm to ∼0.4−0.6 at 13 μm. Globally, the visibility curve is higher for the observation of the 02/06/2004 than for the one of the observations of the 04/02/2004 although their corresponding projected baselines lengths are not very different.

The PAHs leave their mark on the visibility curves. Despite the differences in the mean visibility levels, the decrease in visibility correspond to a full dilution by the flux emitted in the features, as estimated in the previous section. This implies that the emitting regions are fully resolved, i.e. that their correlated flux is close to zero. Given the error bars, we estimate that the bulk of the PAH emitting regions is larger than 50−70 mas (assuming a Gaussian distribution).

4. Discussion

4.1. PAHs

It is not possible to get a hint of geometrical asymmetry in the PAH signals because they are over-resolved with a 46 m baseline (their visibility equals 0). This means that the lower limit of the bulk of their line forming region is at least 50−70 mas. In an other hand, it is possible to place some constraints on the size of the PAH feature forming regions, based on the study of the fluxes recorded by ISO and MIDI

Strong 7.9 μm and 8.6 μm bands and a weaker 11−14 μm plateau are observable in the MIDI spectras whereas the balance of the flux between these two bands in the ISO spectrum is markedly different (see Fig. 3).

The large difference in beam sizes between the two instruments offers a good opportunity to see the effect of an increasing ionizing environment on the behavior of the PAH bands (as suggested in Molster et al. 1996).

The PAH bands from 7 to 9 μm (C−C modes) behave generally in a decoupled way compared to the 3 μm and 11−14 μm plateau (out-of-plane C−H modes). This plateau is attributed to a blend of many bands due to deformation modes of large and *mostly neutral* PAH molecules (Hony et al. 2001; Verstraete et al. 2001; Matsuura et al. 2004). In particular Joblin et al. (1996) interpreted the variations of the 8.6 and 11.3 μm bands in terms of ionization state effects on the CH bending mode intensities, the PAHs being positively charged in regions of high UV excitation. Particularly, the increase of the [8.6]/[11.3] ratio is interpreted as an increase in the ionization of the PAHs. The marked decrease of the 11.3 μm feature in the spectrum while the contribution of 7.9 and 8.6 μm remains more or less stable favors the interpretation that these latter bands are emitted by PAH cations ionized by the direct flux of the post-AGB star and thus which are at a close distance to the star, in the polar axes. Such a behavior is also particularly evident in the case of the PN CPD-56°8032 harboring a Wolf-Rayet star reported by Chesneau et al. (2006).

4.2. Continuum geometry

With only a small number baselines, we can only obtain an estimate of the extension of the emitting regions assuming a spherical geometry. Assuming a Gaussian distribution of flux, the MIDI angular diameters at 13 μm are 24 ± 2 mas and 27 ± 2 mas for the 38° and the 71° baselines, respectively. These angular diameters are impressively close to the one inferred from VINCI measurements, of 22 ± 1.4. This means that the bulk of the near-IR and mid-IR fluxes is located almost in the same physical region. This is a strong argument for the "puffed-up" inner rim, the highly optically thick model ($\tau \geq 10^4$) proposed in Dominik et al. (2003). The estimated Gaussian *FWHM*s from each visibility are also markedly stable from 8 μm to 13 μm, in line with the previous argument, and suggesting that the Gaussian model for the flux distribution at these wavelength is probably close to reality.

It is of interest to know whether the position angles of the projected baselines were aligned with a particular direction in the frame of the HR 4049 binary system for which the dust is supposed to be trapped within a circumbinary disk, althought the observational evidence remains scarce. In that context, polarization measurements (and in particular the position angle ones) are usually the best source of information, yet the case of HR 4049 is complex owing to the time variability of the polarized signal.

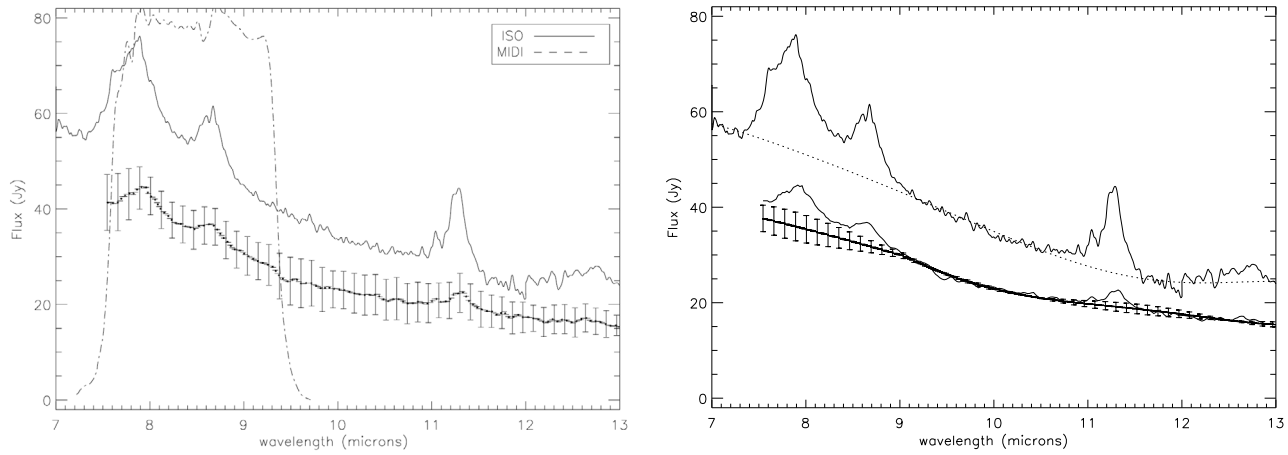

Fig. 2. *Left*: the MIDI spectrum of HR 4049 (lower solid with error bar) is shown in comparison to the ISO one (upper solid). These spectra are calibrated by the spectral template of HD 139127 by Cohen et al. (1999). The bandpass of the N8.7 filter, used for the acquisition files is superimposed (dash-dotted lines). *Right*: the continuum (dotted line) for each spectrum is fitted by a polynomial equation. The error bar of the MIDI continuum is given by the standard deviation of three different fits (see Sect. 3).

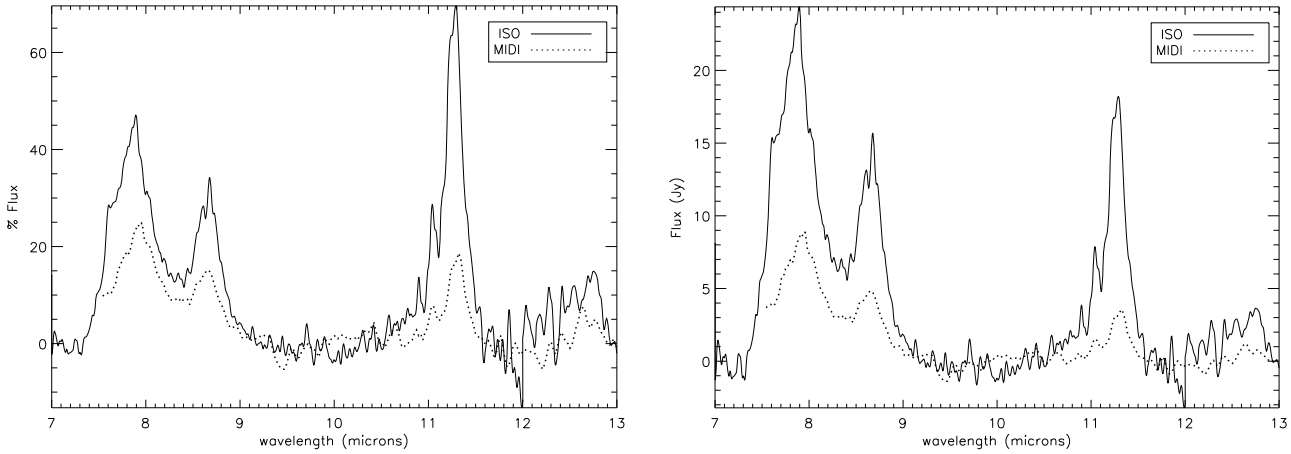

Fig. 3. *Left*: the result of the ratio of ISO and MIDI spectra with their respective continuum, shifted to zero. This show their differences, mainly due to PAH Bands. *Right*: difference between the spectra and their continuum, showing the total amount of flux present in the spectral bands.

The VINCI observations appear to point to a spherical geometry, in apparent contradiction to the disk hypothesis. However, owing to the limited spatial frequency covered, the disk hypothesis is not excluded by VINCI data, bearing in mind that the disk vertical extent can be large in the frame of the model developed by Dominik et al. (2003), and that the inclination is close to 60° in their model. The trend of the VINCI angular dimensions estimated from the K band visibilities obtained with the 8 m baselines (from PA = 53° to 82°) suggests a major axis around 80−100°. Note that the smaller *FWHM* derived at PA ∼ 105° in Antoniucci et al. (2005) is based on a 24 m and not a 8 m baseline. This discrepancy is most probably not due to an effect of the position angle, but a direct consequence of the non-Gaussian flux distribution of the source at this wavelength. This discrepancy can only be interpreted in the frame of a full radiative transfer model of the source.

Johnson et al. (1999) presented spectropolarimetric observations in the UV (space observations with the WUPPE experiment) and the visible (from the ground). They report a high degree of polarization in the UV, with a change of 90° in the position angle around 0.2 μm that was interpreted in the frame of a bipolar structure. These observations clearly define two perpendicular directions: the "UV one" close to 0 degree[2] and the ones in the red around 90−110 degree. We putatively can attribute part of the polarization in the UV to PAH in the polar direction[3], and the other polarization to bigger dust grains associated with the dusty structure in the red. The MIDI visibilities suggest that the dust envelop is more elongated at a position angle of 70° than at 40°. This is in agreement with the trend seen in the VINCI data.

5. Conclusion

We have presented high spatial resolution observations of the dusty environment of HR 4049, consisting of MIDI/VLTI observations obtained with MIDI/VLTI and the UTs.

We found that the bulk of the PAH line forming region is at least 50−70 mas in size and estimated the size of the

[2] The position angle reported by Johnson et al. (1999) is 90−100° which implies, under the hypothesis of an optically thin medium, that the main axis of the scattering structure is at a position angle of 0−10°.

[3] In line with the conclusions of Molster et al. (1996) suggesting, based on the absence of a plateau in the N band features, that the PAHs in HR 4049 are relatively small (at least smaller than 50−100 atoms).

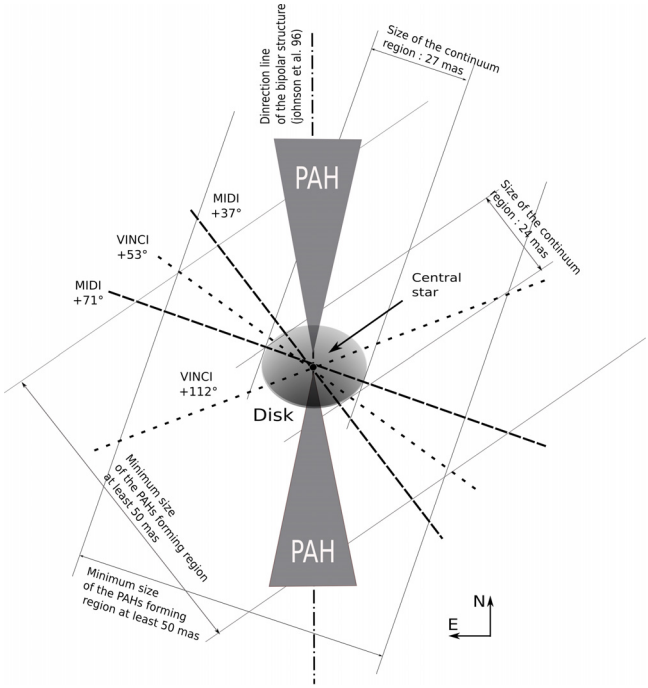

Fig. 4. Sketch of HR 4049: the central star (the circle in the center) is surrounded by a thick disk (the ellipsoid) whose directions are approximately determined from polarization measurements of Johnson et al. (1999). Two PAH jets are represented in the polar regions above the disk. The VLTI baselines are also represented, with the MIDI baselines in dashed lines and the extrema of the VINCI ones in dotted lines. The baselines are not scaled in length. The size of the disc and the minimum size of the PAH forming region as given by the MIDI data are drawn in pale-grey.

continuum-emitting regions at 13 μm as 24±2 mas and 27±2 mas for the 38° and the 71° baselines. Figure 4 shows the disc (with the two sizes given by the MIDI data) and the two PAH jets (with the minimum size of the PAH forming region for each of the MIDI baselines) of HR 4049.

This bright object ($F_{12\ \mu m}$ = 48.25 Jy) can also be studied with a large number of baselines with MIDI thanks to the 1.8 m VLT Auxiliary Telescopes. The parameters extracted in this paper made use of a limited sample of interferometric measurements based on baselines orientated along the major axis of the disk. Observations performed with baselines aligned close to the minor axis should provides higher visibilities changing more rapidly with orientation. It should also be possible to use a set of short VLTI baselines (16−32 m) to better determine the location and the rough geometry of the PAH emitting regions, and detect differences between the spatial distribution of the 7.9, 8.6 and 11.3 features. A similar study could be carried out on the famous Red Rectangle ($F_{12\ \mu m}$ = 421.6 Jy) which would represent a good complement to the study of PAHs performed in the visible at larger scales.

References

Antoniucci, S., Paresce, F., & Wittkowski, M. 2005, A&A, 429, L1
Bakker, E. J., Lambert, D. L., Van Winckel, H., et al. 1998, A&A, 336, 263
Bakker, E., Meisner, J., Percheron, I., et al. 2004, SPIE, 5491, 35
Beintema, D. A., van den Ancker, M. E., Molster, et al. 1996, A&A, 315, L369
Chesneau, O., Verhoelst, T., Lopez, B., et al. 2005, A&A, 435, 563
Chesneau, O., Collioud, A., De Marco, O., et al. 2006, A&A, 455, 1009
Cohen, M., Walker, R. G., Carter, B., et al. 1999, AJ, 117, 1864
Dominik, C., Dullemond, C. P., Cami, J., & van Winckel, H. 2003, A&A, 397, 595
Hony, S., Van Kerckhoven, C., Peeters, E., et al. 2001, A&A, 370, 1030
Jaffe, W. 2004, Proc. SPIE, 5491, 715
Joblin, C., Tielens, A. G. G. M., Geballe, T. R., & Wooden, D. H. 1996, ApJ, 460, L119
Johnson, J. J., Anderson, C. M., Bjorkman, K. S., et al. 1999, MNRAS, 306, 531
Leinert, C., Graser, U., Waters, L. B. F. M., et al. 2003a, Proc. SPIE, 4838, 893
Leinert, C., Graser, U., Przygodda, F., et al. 2003b, Ap&SS, 286, 73
Leinert, C., van Boekel, R., Waters, L. B. F. M., et al. 2004, A&A, 423, 537
Matsuura, M., Zijlstra, A. A., Molster, F. J., et al. 2004, ApJ, 604, 791
Molster, F. J., van den Ancker, M. E., Tielens, A. G. G. M., et al. 1996, A&A, 315, L373
Ohnaka, K., Driebe, T., Weigelt, G., & Wittkowski, M. 2007, A&A, 466, 1099
Ratzka, T., 2005, Ph.D. Thesis, Ruprecht-Karls-Universität Heidelberg
Ratzka, T., Leinert, Ch., Henning, Th., et al. 2007, A&A, 471, 173
Van Winckel, H., Lloyd Evans, T., Reyniers, M., Deroo, P., & Gielen, C. 2006, Mem. Soc. Astron. Ital., 77, 943
Verstraete, L., Pech, C., Moutou, C., et al. 2001, A&A, 372, 981
Vijh, U. P., Witt, A. N., & Gordon, K. D. 2005, ApJ, 619, 368